ARCHIVES OF ELECTRICAL ENGINEERING VOL. 68(1), pp. 77–90 (2019)

DOI 10.24425/aee.2019.125981

Research on the influence of rotational speed on the performance of high-speed permanent-magnet generator

HONGBO QIU, YANQI WEI, XI FANG ZHAO, CUNXIANG YANG, RAN YI

School of Electrical and Information Engineering, Zhengzhou University of Light Industry
Zhengzhou, Henan, China
e-mail: zhaoxifang1993@163.com

(Received: 31.07.2018, revised: 16.10.2018)

Abstract: When the machine is at high speed, serious problems occur, such as high frequency loss, difficult thermal management, and the rotor structural strength insufficiency. In this paper, the performances of two high-speed permanent magnet generators (HSPMGs) with different rotational speeds and the same torque are compared and analyzed. The two-dimensional finite element model (FEM) of the 117 kW, 60 000 rpm HSPMG is established. By comparing a calculation result and test data, the accuracy of the model is verified. On this basis, the 40 kW, 20 000 rpm HSPMG is designed and the FEM is established. The relationship between the voltage regulation sensitivity and power factor of the two HSPMGs is determined. The influence mechanism of the voltage regulation sensitivity is further revealed. In addition, the air-gap flux density is decomposed by the Fourier transform principle, and the influence degree of different harmonic orders on the HSPMG performance is determined. The method to reduce the harmonic content is further proposed. Finally, the method to improve the HSPMG overload capacity is obtained by studying the maximum power. The research showed that the HSPMG at low speed (20 000 rpm) has high sensitivity of the voltage regulation, while the HSPMG at high speed (60 000 rpm) is superior to the HSPMG at low speed in reducing the harmonic content and increasing the overload capacity.

Key words: high-speed permanent-magnet generator (HSPMG), harmonic content, maximum power, overload capacity, voltage regulation

1. Introduction

The high-speed permanent-magnet generator has the advantages of small volume, high reliability, high efficiency, the small moment of inertia and fast dynamic response [1–4]. It has a good application prospect in the fields of aerospace, a vacuum pump and flywheel energy storage [5–7]. It is attracting more and more researchers' attention.

In order to reduce the stator core loss and external rectifier loss of the generator, it is necessary to minimize the operating frequency at a given rotational speed. Therefore, the number of poles chosen by the HSPMG is usually 2. Especially when the pole numbers is 2, the length of the stator end windings will even be the same as the stator straight line winding. In addition, when the generator runs at high speed, its frequency will exceed the first natural frequency [8]. When the rotor is overlong, the mechanical strength of the rotor is decreased, and the rotor will be deformed. However, the Gramme ring windings [9] can effectively shorten the rotor length for better stiffness under high-speed rotation. The Gramme ring windings are shown in Fig. 1(a). One side of the Gramme ring winding is embedded in the stator core slot, and the other side is placed on the back of the stator yoke.

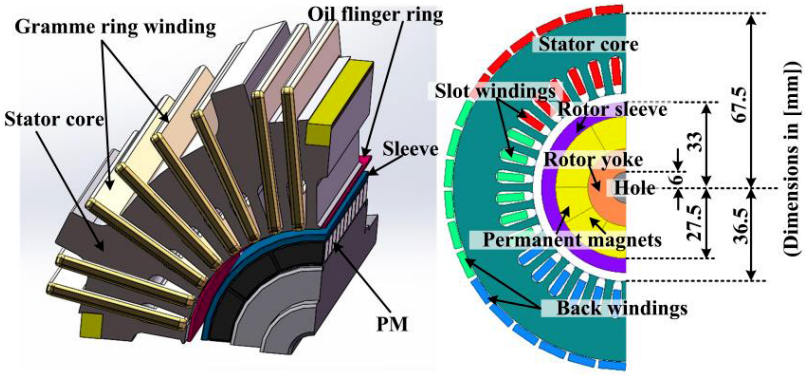

(a) (b)

Fig. 1. The structure of the HSPMG (a); the two-dimensional FEM of the HSPMG (b)

In recent years, many researchers aim to the research of machine speed. Some scholars have put forward a new method for machine speed detection [10] and instantaneous speed measurement [11]. In addition, some scholars adjust the machine speed by current modulation [12] and a back-propagation algorithm [13]. Furthermore, speed is very important for machine performance research. The fast-filtering algorithm can be implemented based on speed jitter [14]. In order to achieve the purpose of torque control, speed can be used as a feedback signal in torque control [15]. At the same time the speed can also be used as a control variable of the control strategy, which provides a new idea for the research of wind turbine power control strategies [16]. It is worth mentioning that no similar study on the differences of the HSPMG performance at different speeds has been found in many literatures.

In order to provide a theoretical basis for speed determination in the HSPMG design process, the performances of two HSPMGs with different rotational speeds but the same torque are compared and analyzed in this paper. The parameters, experimental platform, calculation result and test data of the HSPMG are introduced in the second section. In the third section, the harmonic content, the overload capacity and the relationship between the voltage regulation sensitivity and power factor are compared and analyzed. Through the above research, some useful conclusions are obtained, which could provide the basis for the further research on the HSPMG.

2. Parameters and model of the HSPMG

2.1. Parameters and model

In this paper, two HSPMGs with the same rated torque and a rated speed of 20 000 rpm and 60 000 rpm were analyzed and compared. The permanent magnet adopts radial magnetization and it is mounted on the rotor yoke surface in an axially segmented way. The axial segmentation is designed to reduce the eddy current loss [14]. However, the high speed of the HSPMG leads to a great rotor surface linear velocity. It means that the rotor surface has a great centrifugal force. Therefore, it is necessary to add a sleeve on the rotor surface to protect the permanent magnet.

In addition, the stator adopts a closed cavity oil cooling mode to increase the heat dissipation of the Gramme ring winding and stator core. Fig. 2 shows a stator end and a prototype of the HSPMG. The basic parameters of the two HSPMG are shown in Table 1. Based on the actual structure of the prototype, two-dimensional finite element models of the HSPMG are established, as shown in Fig. 1(b).

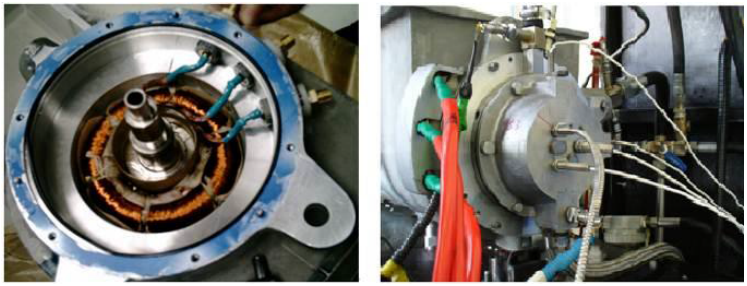

Fig. 2. Prototype and stator end of the HSPMG

Table 1. The parameters of the two generators

Parameters	Value		Parameters	Value
Rated power (kW)	60 000 rpm	117	**Rated voltage (V)**	670
	20 000 rpm	40	**Pole number**	2
Number of turns	60 000 rpm	2	**Core length (mm)**	275
	20 000 rpm	6	**Rotor type**	PM
Frequency (Hz)	60 000 rpm	1 000	**Stator outer diameter (mm)**	135
	20 000 rpm	1 000/3	**Stator inner diameter (mm)**	72
Slot number	36		**Rotor outer diameter (mm)**	66

In order to simplify the calculation, three hypotheses are made in this paper [17–18]:

1. It is assumed that the magnetic field is uniformly distributed along the axial direction in the analysis of a two-dimensional transient field. It means that current density vector $\boldsymbol{J}$ and magnetic potential vector $\boldsymbol{A}$ only have the component in the z-direction, $\boldsymbol{J} = \boldsymbol{J}_z$, $\boldsymbol{A} = \boldsymbol{A}_z$.

2. Materials are isotropic. The permeability of the material is constant and the variation of the permeability with the change of the temperature is ignored.
3. The influence of a displacement current is assumed to be ignored. It is considered that the electromagnetic field of the generator is a nonlinear constant electromagnetic field.

Based on the above assumptions and electromagnetic field theory, the boundary value equation of a two-dimensional transient electromagnetic field generator is established by $\boldsymbol{A}_z$ in this paper [19]:

$$\begin{cases} \Omega: \dfrac{\partial^2 \boldsymbol{A}_z}{\partial x^2} + \dfrac{\partial^2 \boldsymbol{A}_z}{\partial y^2} = -\mu \boldsymbol{J}_z + \mu\sigma \dfrac{\partial \boldsymbol{A}_z}{\partial t} \\ \Gamma_1: \boldsymbol{A}_z = 0 \\ \Gamma_2: \dfrac{1}{\mu_1}\dfrac{\partial \boldsymbol{A}_z}{\partial n} - \dfrac{1}{\mu_2}\dfrac{\partial \boldsymbol{A}_z}{\partial n} = \boldsymbol{J}_s \end{cases}, \tag{1}$$

where: Ω is the calculation region, $\boldsymbol{A}_z$ and $\boldsymbol{J}_z$ are the magnetic vector potential and the source current density in the z-axial component, respectively, $\boldsymbol{J}_s$ is the equivalent face current density of the PM, σ is the conductivity, Γ_1 is the parallel boundary condition, Γ_2 is the PM boundary condition, and μ_1 and μ_2 are relative permeability values.

In this paper, the electromagnetic field of an HSPMG is analyzed by the field-circuit coupling method. The external circuit is shown in Fig. 3. In Fig. 3, region A is the winding resistance and leakage inductance, region B is the load resistance and inductance.

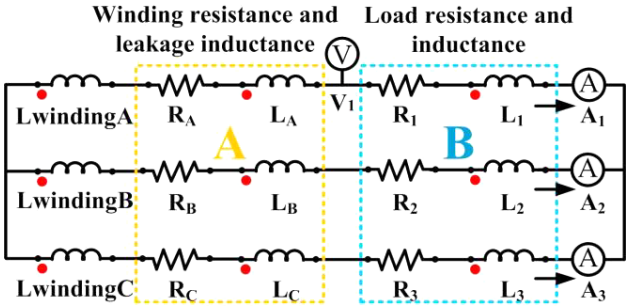

Fig. 3. External circuit of the HSPMG

2.2. Experimental testing and data comparison

The HSPMG prototype was tested to verify the correctness of the analysis results. The experimental test platform and the experiment equipment are shown in Fig. 4. The terminal voltage and the armature current are obtained when the generator is running at a speed of 6 000, 8 000 and 10 000 rpm, respectively. The experimental data and the finite element model calculated results are shown in Table 2. In Table 2, the terminal voltage is line voltage and the armature current is line current. And the terminal voltage and the armature current are effective value.

From the data in Table 2, there is little difference by comparing the experimental data with the model calculation results. The maximum difference of the terminal voltage between the test data and the calculated results is 0.7 V, and the deviation is not more than 1.13%. The maximum

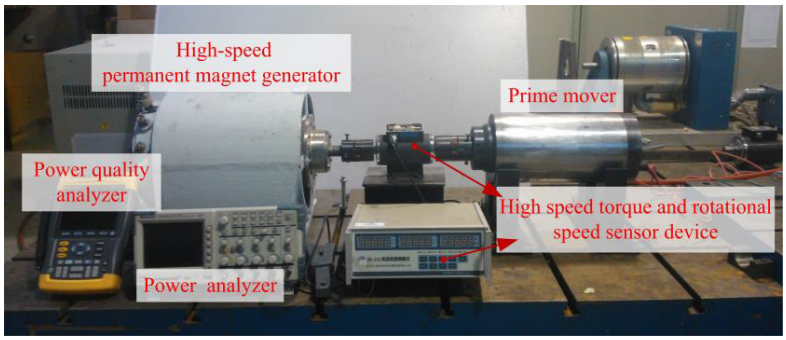

Fig. 4. Test platform of the HSPMG

Table 2. Comparison of the test data and the finite element model calculated results

Speed (rpm)	Terminal voltage		Deviation	Armature current		Deviation
	Calculated results	Test data		Calculated results	Test data	
6 000	39.9 V	39.6 V	0.75%	14.5 A	14.4 A	0.69%
8 000	53.1 V	53.7 V	1.13%	18.3 A	18.5 A	1.09%
10 000	65.8 V	65.1 V	1.06%	22.4 A	22.1 A	1.34%

difference of the armature current between the test data and the calculated results is 0.3 A and the deviation is not more than 1.34%. Through the above data, the accuracy of the finite element model has been verified.

Fig. 5 shows the comparisons of the EMF waveforms obtained from the test and the finite element method. It can be seen that the EMF waveforms obtained from the two methods are in agreement. Due to the less harmonic content of the EMF, the waveform is almost sinusoidal.

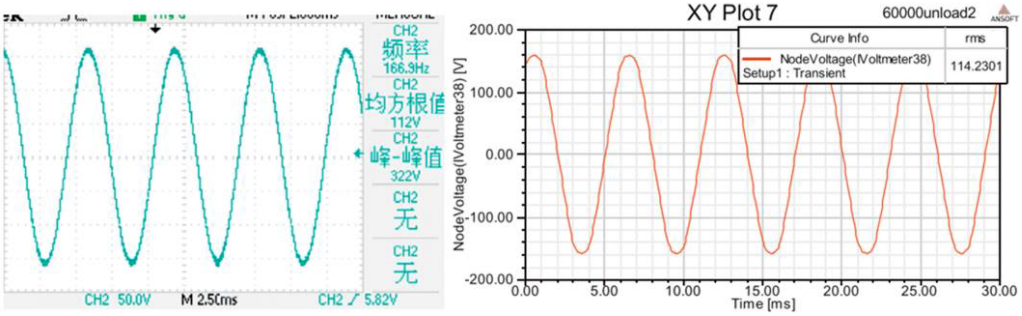

(a) (b)

Fig. 5. The test EMF waveform (a); The finite element calculated EMF waveform (b)

3. The influence of speed on HSPMG performance

3.1. The influence of speed on the HSPMG voltage regulation

The voltage regulation is an important parameter that reflects the performance of a generator. It is a measure of the ability of a generator to keep a constant voltage at its terminals as load varies. The small voltage regulation leads to small fluctuation of the generator output terminal voltage, so the generator has a better running stability. However, the magnetic field of the PM generator is produced by the PM and not adjustable, which leads to the voltage regulation difficult to change. It can be seen that voltage regulation is an important parameter for studying the differences of the two HSPMGs performance at different speeds.

The voltage regulation is defined by the equation:

$$\Delta U = \frac{E_0 - U}{U_N} \times 100\%, \tag{2}$$

where E_0 is the non-load terminal voltage, U is the load terminal voltage, and U_N is the rated terminal voltage.

The vector diagram of the HSPMG with a resistance-inductive load is shown in Fig. 6.

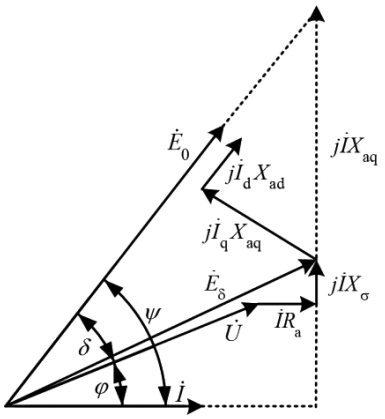

Fig. 6. The vector diagram of the HSPMG with resistance-inductive load

where E_δ is the air-gap synthesis electromotive force, R_a is the armature resistance of each phase, X_σ is the leakage reactance of the generator armature winding, X_{ad} is the direct axis reactance of armature reaction, X_{aq} is the quadrature axis reactance of armature reaction, I is the load current of the generator with inductive, I_d is the direct axis current, I_q is the quadrature axis current, δ is the power angle, φ is the external power factor angle, and ψ is the internal power factor angle.

The following formula can be obtained from Fig. 6.

$$U = \sqrt{E_\delta^2 + I_q^2 X_{aq}^2 \cos^2\psi - I^2 \left(R_a \sin\varphi - X_\sigma \cos\varphi\right)^2} - I\left(R_a \sin\varphi - X_\sigma \cos\varphi\right), \tag{3}$$

$$\psi = \delta + \varphi = \arctan\frac{U\sin\varphi + IX_q}{U\cos\varphi + IR_a}, \tag{4}$$

$$U\sin\delta = I_q X_q + IX_\sigma \cos(\delta+\varphi) - IR_a \sin(\delta+\varphi) = I_q X_q - IR_a \sin(\delta+\varphi). \tag{5}$$

Because the armature resistance of the HSPMG is much less than that of synchronous reactance, it can be neglected. When the armature resistance is not considered, the electromagnetic power will be approximately equal to the armature terminal output power.

$$P = P_{\mathrm{e}} = m\frac{E_0 U}{X_{\mathrm{q}}}\sin\delta, \tag{6}$$

$$U = \frac{PX_{\mathrm{q}}}{mE_0\sin\delta}, \tag{7}$$

where P_{e} is the electromagnetic power, P is the armature terminal output power.

From (5) and (7) we can conclude that, there is a certain connection between the HSPMG output terminal voltage and power angle. Fig. 7 shows the variations of the power angle, voltage and voltage regulation of the two HSPMGs. In Fig. 7, the voltage is obtained by the FEM, and the voltage regulation is calculated by Formula (2). Fig. 7 shows the vector diagram of the two HSPMGs.

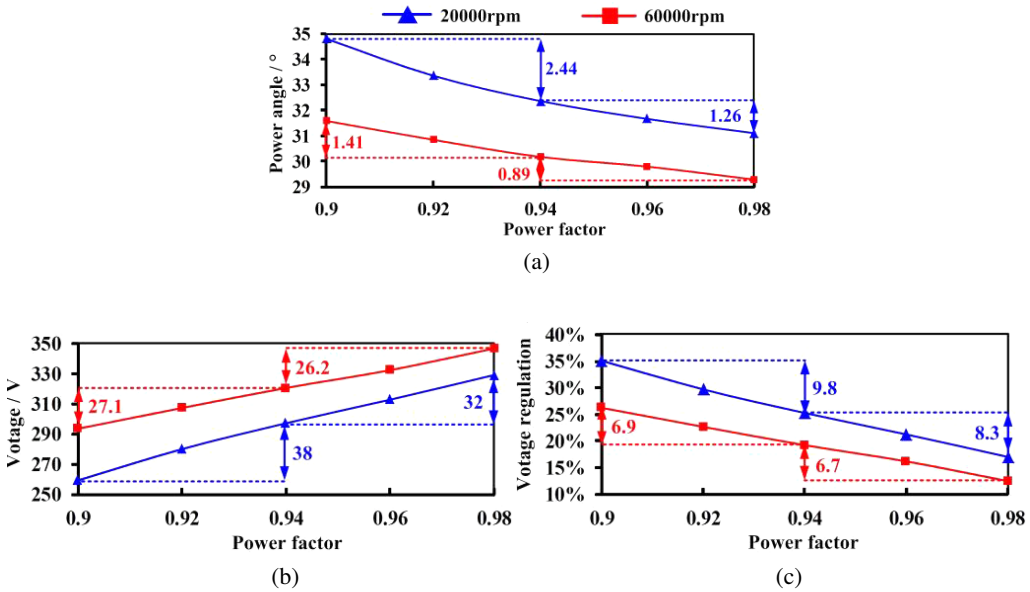

Fig. 7. The power angle variation of the two HSPMGs (a); The voltage variation of the two HSPMGs (b); The voltage regulation variation of the two HSPMGs (c)

According to Fig. 7, under the rated power, the power angle and voltage regulation of the two HSPMGs both decrease with the increase of the power factor. At any power factor the power angle and voltage regulation of the HSPMG at lower speed are higher than those of the HSPMG at higher speed. The variation of the power angle, voltage and voltage regulation is shown in Table 3. In Table 3, range A represents the power factor from 0.9 to 0.94 and range B represents the power factor from 0.94 to 0.98. PA represents the power angle, V represents the voltage, and VR represents the voltage regulation.

Table 3. The variation of the power angle, voltage and voltage regulation

Type	**20 000 rpm**						**60 000 rpm**					
	Range A			Range B			Range A			Range B		
	PA	V	VR	PA	V	VR	PA	V	VR	PA	V	VR
Decrease	2.44°	0 V	9.8%	1.26°	0 V	8.3%	1.41°	0 V	6.9%	0.89°	0 V	6.7%
Increase	0°	38 V	0%	0°	32 V	0%	0°	27.1 V	0%	0°	26.1 V	0%

It can be seen that increasing the power factor significantly reduces the voltage regulation of the HSPMG. In range A, the variation of the HSPMG voltage regulation at low speed is 42% higher than those of the HSPMG at high speed. In range B, the variation of the HSPMG voltage regulation at low speed is 23.9% higher than those of the HSPMG at high speed. Therefore, the voltage regulation is more sensitive to the power factor change when the HSPMG is at low speed. The reason can be obtained from Fig. 8. As shown in Fig. 8, when the same power factor is increased, the variation of the power angle of the HSPMG at low speed is greater. It leads to the output terminal voltage change more obviously, which results in the effect of reducing the voltage regulation better.

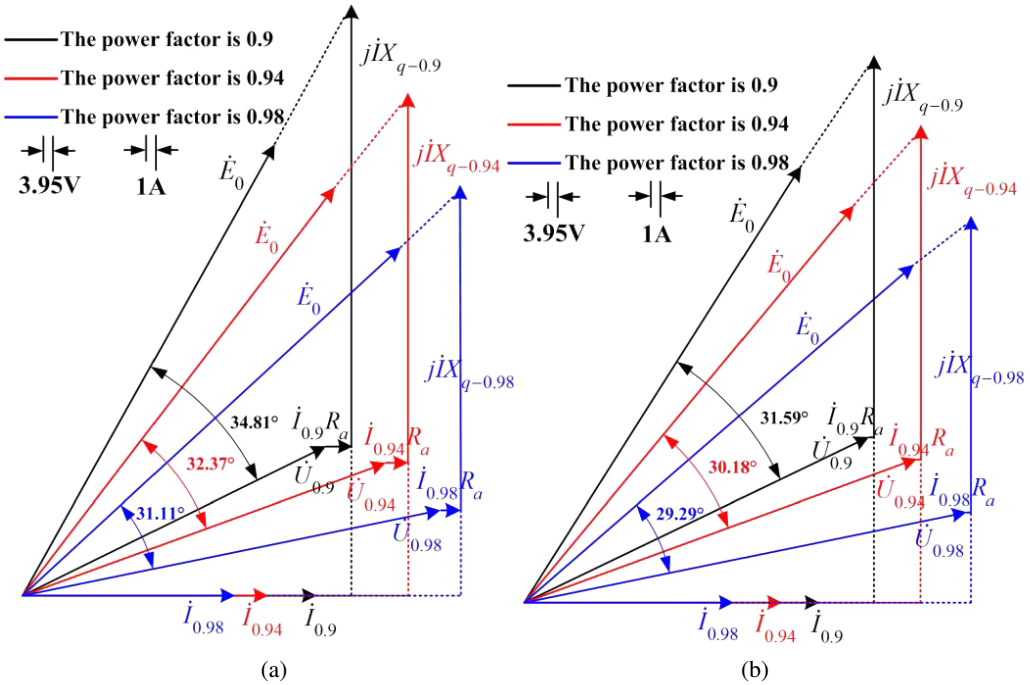

Fig. 8. The vector diagram of HSPMG at 20 000 rpm (a); The vector diagram of HSPMG at 60 000 rpm (b)

3.2. The influence of speed on the HSPMG air-gap flux density

The electromagnetic parameters such as the rotor loss and induction electromotive force depend on the air-gap flux density distribution. Therefore, the air-gap flux density waveform directly affects the generator performance. Because the stator slotting, the air-gap flux density contains more tooth harmonics, which leads to the air-gap flux density waveform serrated obviously.

The harmonics cause the electromagnetic torque fluctuation, which leads to the generator vibration and noise. In addition, the high speed of the HSPMG increases the relative motion between the harmonic magnetic field and the rotor, which increases the eddy current loss and cause heat in the sleeve. Therefore, the harmonics not only reduce the efficiency of the generator, but also lead to the demagnetization of the permanent magnet. It is necessary to study the air-gap flux density.

In addition, the air-gap flux density waveform is obtained based on the FEM. By the Fourier transform principle, the air-gap flux density is decomposed when the power factor of the HSPMG is 0.94 and the speed is 20 000 rpm. The waveform of the air-gap flux density, the waveform of the fundamental and the waveform of the harmonics are shown in Fig. 9.

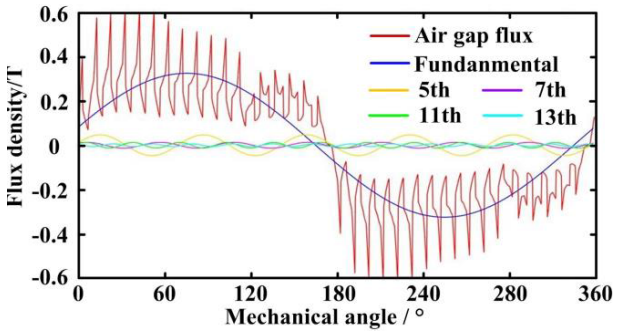

Fig. 9. The waveform of the air-gap flux density, the waveform of the fundamental and the waveform of the harmonics

Because the generator winding is of the Y type, three and three multiples of the harmonics could not flow in the generator, so the 3^{th}, 9^{th} harmonics and so on could be ignored. The data after the decomposition of the air-gap flux density is shown in Fig 10. Fig. 10 is each harmonic amplitude of the two HSPMGs under different power factors. As shown in Fig 10, the amplitudes of the 5^{th}, 11^{th} and other harmonics gradually decrease with the increase of the power factor, while the amplitudes of the fundamental and 7^{th} harmonics gradually increase. Fig. 11 shows the ratios of the 5^{th}, 7^{th} and 11^{th} harmonics to fundamental under different power factors. The ratios of the harmonics to fundamental of the two HSPMGs and the multiple relationships are shown in Table 4.

As shown in Table 4, the ratio of the 7^{th} harmonic to fundamental of the two HSPMGs is the same, which indicates that the influences of the 7^{th} harmonic on the two HSPMGs performance are the same. However, the ratios of the 5^{th} and 11^{th} harmonics to fundamental of the HSPMG at low speed are higher than those of the HSPMG at high speed. Especially when the power factor is 0.9, the 11^{th} harmonic to fundamental of the HSPMG at low speed is 2.31 times of the HSPMG at

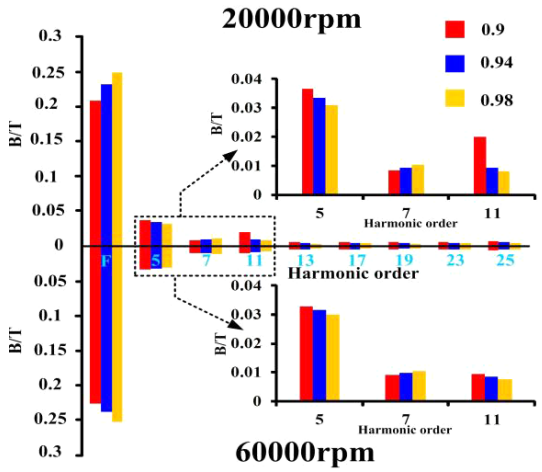

Fig. 10. Harmonic amplitudes of the two HSPMGs under different power factor

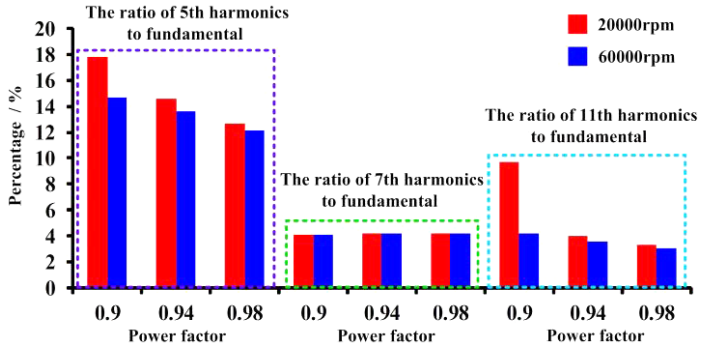

Fig. 11. The ratio of harmonics to fundamental of the two HSPMGs

Table 4. The ratios of harmonic to fundamental of the two HSPMGs and the multiple relationships

Harmonic order	**5th**			**7th**			**11th**		
Power factor	0.9	0.94	0.98	0.9	0.94	0.98	0.9	0.94	0.98
20 000 rpm	17.8%	14.6%	12.7%	4.2%	4.2%	4.2%	9.7%	4%	3.3%
60 000 rpm	14.7%	13.6%	12.1%	4.2%	4.2%	4.2%	4.2%	3.6%	3%
Multiple relationship	1.21	1.07	1.05	1	1	1	2.31	1.11	1.1

high speed. Therefore, the 5th and 11th harmonics are the main reasons leading to the differences of the two HSPMGs performance.

When the power factor is 0.9, 0.94 and 0.98, compared with the HSPMG at low speed, the ratio of the 5th harmonic to fundamental of the HSPMG at high speed decreases by 4.3%, 1% and 0.4% respectively, and the ratios of the 11th harmonic to fundamental of the HSPMG at high speed decrease by 5.5%, 0.6% and 0.3% respectively. Therefore, in the design process of the

HSPMG, when the power factor is determined, the higher the speed of the HSPMG is designed, the more favorable it is to reduce the harmonic content.

In addition, when the speed of the HSPMG are 20 000 rpm and 60 000 rpm, compared with that when the power factor is 0.9, the ratio of the 5^{th} harmonic to fundamental of a power factor of 0.98 decreases by 5.1% and 2.6%, and the ratio of the 11^{th} harmonic to fundamental of a power factor of 0.98 decreases by 6.4% and 1.2%. Therefore, in the design process of the HSPMG, when the speed is determined, the lower the power factor of the HSPMG is designed, the more favorable it is to reduce the harmonic content.

3.3. The influence of speed on the generator maximum power

The maximum power reflects the overload capacity of the generator. At the moment of overloading, it is usually hoped that the generator will send out enough power to maintain the power grid stable. Therefore, when the generator is designed, its maximum power is always as large as possible. In order to analyze the overload capacity of the two HSPMGs simply, the overload rate (OLR) is defined as follows:

$$\mathrm{OLR} = \frac{P_{\max} - P}{P} \cdot 100\%, \tag{8}$$

where $P_{\max}$ is the maximum power, $P$is the rate power.

The maximum powers of the two HSPMGs under a different power factor are obtained by the FEM. The maximum power and OLR of the two HSPMGs are shown in Table 5.

Table 5. The maximum power and OLR of the two HSPMGs

Power factor	**60 000 rpm**		**20 000 rpm**	
	P_{max}	**OLR**	**P_{max}**	**OLR**
0.9	131.1 Kw	12.05%	41.3 Kw	3.25%
0.92	138 Kw	17.9%	43.4 Kw	8.5%
0.94	146.1 Kw	24.9%	45.7 Kw	14.25%
0.96	155.8 Kw	33.2%	48.6 Kw	21.5%
0.98	169.2 Kw	44.6%	52.5 Kw	31.25%

As shown in Table 5, when the speed of the HSPMG are 20 000 rpm and 60 000 rpm, compared with that when the power factor is 0.9, the OLR of a power factor of 0.98 increases by 32.55% and 30%. Therefore, in the design process of the HSPMG, when the speed is determined, the higher the power factor of the HSPMG is designed, the more favorable it is to increase the OLR.

In addition, at any power factor, the OLR of the HSPMG at high speed is significantly higher than that of the HSPMG at low speed. When the power factor is 0.9, 0.94 and 0.98, compared with the HSPMG at low speed, the OLR of the HSPMG at high speed increases by 8.8%, 10.65% and 13.35% respectively. Therefore, in the design process of the HSPMG when the power factor is determined, the higher the speed of the HSPMG is designed, the more favorable it is to increase the OLR.

4. Conclusions

In order to compare and analyze the performances of the two HSPMGs with different rotational speeds but the same torque, the voltage regulation, air-gap flux density and maximum power of the two HSPMGs at low speed (20 000 rpm) and high speed (60 000 rpm) are studied. The conclusions are as follows:

1. At any speed, increasing the power factor can reduce the HSPMG voltage regulation. However, the voltage regulation is more sensitive to the power factor change when the HSPMG is at low speed. Especially when the power factor is increased from 0.9 to 0.94, the variation of the HSPMG voltage regulation at low speed is 42% higher than those of the HSPMG at high speed. Therefore, changing the power factor is an effective way to reduce the voltage regulation when the HSPMG is at low speed.
2. By the Fourier decomposition, the ratio of the 7^{th} harmonic to fundamental of the two HSPMGs is the same. However, the ratios of the 5^{th} and 11^{th} harmonics to fundamental of the HSPMG at low speed are higher than those of the HSPMG at high speed. Especially when the power factor is 0.9, the 11^{th} harmonic to fundamental of the HSPMG at low speed is 2.31 times of the HSPMG at high speed. Therefore, the 5^{th} and 11^{th} harmonics are the main reasons leading to the differences of the two HSPMGs performance.
3. In the design process of the HSPMG, when the power factor is determined, the higher the speed of the HSPMG is designed, the more favorable it is to reduce the harmonic content. Especially when the power factor is 0.9, compared with the HSPMG at low speed, the ratios of the 5^{th} and 11^{th} harmonics to fundamental of the HSPMG at high speed decrease by 4.3% and 5.5%.
4. In the design process of the HSPMG, when the speed is determined, the lower the power factor of the HSPMG is designed, the more favorable it is to reduce the harmonic content. Especially when the speed of the HSPMG is 20 000 rpm, compared with that when the power factor is 0.9, the ratios of the 5^{th} and 11^{th} harmonics to fundamental of the power factor of 0.98 decreases by 5.1% and 6.4%.
5. In the design process of the HSPMG, when the speed is determined, the higher the power factor of the HSPMG is designed, the more favorable it is to increase the OLR. Especially when the speed of the HSPMG is 20 000 rpm, compared with that when the power factor is 0.9, the OLR of a power factor of 0.98 increases by 32.55%. In addition, when the power factor is determined, the higher the speed of the HSPMG is designed, the more favorable it is to increase the OLR. Especially when the power factor is 0.98, compared with the HSPMG at low speed, the OLR of the HSPMG at high speed increases by 13.35%.

Acknowledgements

This work was supported in part by the National Natural Science Foundation of China under Grant 51507156, in part by the University Key Scientific Research Programs of Henan province under Grant 17A470005, in part by the Doctoral Program of Zhengzhou University of Light Industry under Grant 2014BSJJ042, in part by the Major Science and Technology Special Projects of Henan Province under Grant 16110021160, and in part by the Foundation for Key Teacher of Zhengzhou University of Light Industry.

References

[1] Jang S.-M., Koo M.-M., Park Y.-S., Choi J.-Y., Lee S.-H., *Characteristic analysis of permanent magnet synchronous machines under different construction conditions of rotor magnetic circuits by using electromagnetic transfer relations*, IEEE Transactions on Magnetics, vol. 47, no. 10, pp. 3665–3668 (2011).

[2] Cho H.W., Myeong S., Choi S.-K., *A design approach to reduce rotor losses in high speed permanent magnet machine for turbocompressor*, IEEE Transactions on Magnetics, vol. 42, no. 10, pp. 3521–3523 (2006).

[3] Li W., Qiu H., Zhang X. *et al.*, *Analyses on electromagnetic and temperature fields of super high-speed permanent-magnet generator with different sleeve materials*, IEEE Transactions on Industrial Electronics, vol. 6, no. 6, pp. 3056–3063 (2014).

[4] Zhang Y., McLoone S., Cao W.P., *Electromagnetic loss modeling and demagnetization analysis for high speed permanent magnet machine*, IEEE Transactions on Magnetics, vol. 54, no. 3, ASN 8200405 (2018).

[5] Chen D., Feng M., *The influence of magnetic field on losses of high-speed permanent magnet motor*, Proceedings of 2016 IEEE Int. Conf. Mechatronics and Automation, Harbin, Heilongjiang, China, pp. 27–31 (2016).

[6] Hong D.K., Woo B.C., Lee J.Y., *Ultra high speed motor supported by air foil bearings for air blower cooling fuel cells*, IEEE Transactions on Magnetics, vol. 48, no. 2, pp. 871–874 (2012).

[7] Chen D., Feng M., *The influence of magnetic field on losses of high-speed permanent magnet motor*, Proceedings of 2016 IEEE Int. Conf. Mechatronics and Automation, Harbin, Heilongjiang, China, pp. 27–31 (2016).

[8] Silong Li, Yingjie Li, Wooyoung Choi, Bulent Sarlioglu, *High Speed Electric Machines – Challenges and Design Considerations*, IEEE Trans. Transport. Elect., vol. 2, no. 1, pp. 2–13 (2016).

[9] Jian ning Dong, Yun kai Huang, Long Jin, Bao cheng Guo, Heyun Lin, Jiyong Dong, Ming Cheng, Hui Yang, *Electromagnetic and Thermal Analysis of Open-Circuit Air Cooled High-Speed Permanent Magnet Machines with Gramme Ring Windings*, IEEE Transactions on Magnetics, vol. 50, no. 11, ASN 8104004 (2014).

[10] Gao Z., Turner L., Colby R.S., Leprettre B., *A Frequency Demodulation Approach to Induction Motor Speed Detection*, IEEE Transactions on Industrial Applications, vol. 47, no. 4, pp. 1632–1642 (2012).

[11] Sun Yiquan, Zhang Yingtang, Li Zhining, Cheng Lijun, *Design on Instantaneous Rotational Speed Measuring Device of Engine*, 2011 International Conference on Instrumentation, Measurement, Computer, Communication and Control, Beijing, China, pp. 126–129 (2011).

[12] Puu-An Juang, Da-Wei Gu, *Speed Control of a New Disc-Type Ultrasonic Motor by Using Current Controller*, IEEE Trans. Pow. Elect., vol. 21, no. 1, pp. 219–224 (2012).

[13] Lazhar Ben-Brahim, Susumu Tadakuma, Alper Akdag, *Speed Control of Induction Motor Without Rotational Transducers*, IEEE Transactions on Industrial Applications, vol. 35, no. 4, pp. 844–850 (1999).

[14] Nerat M., Vrancic D., *A Novel Fast-Filtering Method for Rotational Speed of the BLDC Motor Drive Applied to Valve Actuator*, IEEE/ASME Transactions on Mechatronics, vol. 21, no. 3, pp. 1479–1486 (2016).

[15] Mingfu Liao, Li Dong, Lu Jin, Siji Wang, *Study on Rotational Speed Feedback Torque Control for Wind Turbine Generator System*, 2009 International Conference on Energy and Environment Technology, Guilin, Guangxi, China, pp. 16–18 (2009).

[16] Lucian Mihet-Popa, Frede Blaabjerg and Ion Boldea, *Wind Turbine Generator Modeling and Simulation Where Rotational Speed is the Controlled Variable*, IEEE Transactions on Industrial Applications, vol. 40, no. 1, pp. 3–10 (2004).

[17] Weili L., Jing W., Xiaochen Z., Baoquan K., *Loss calculation and thermal simulation analysis of high-speed PM synchronous generators with rotor topology*, Proceedings of 2010 Int. Conf. Com-puter Application and System Modeling (ICCASM 2010), Taiyuan, pp. V14–612–V14–616 (2010).

[18] Houzhou G., Han L., Nanfan Z. *et al*., *3D loss and heat analysis at the end region of 4-poles 1150 MW nuclear power turbine generator*, Archives of Electrical Engineering, vol. 63, no. 1, pp. 47–61 (2014).

[19] Weili Li, Xiaochen Zhang, Shukang Cheng, Junci Cao, *Thermal Optimization for a HSPMG Used for Distributed Generation Systems*, IEEE Transactions on Industrial Electronics, vol. 60, pp. 474–482 (2013).

[20] Wu Q., Xiong H., Liu L., Meng G., Li H., Zhou L., *Research on voltage regulation of a permanent magnet generator*, Proceedings of 2011 International Conference on Electrical and Control Engineering, Yichang, China, pp. 4935–4937 (2011).